Received 18 October 2015
Revised 27 November 2015
Accepted 29 November 2015

Web-based GIS technologies for monitoring and analysis of spatio-temporal processes

Valery Gitis, Alexander Derendyaev and Arkady Weinstock
The Institute for Information Transmission Problems, Russian Academy of Science, Moscow, Russian Federation

Abstract

Purpose – This paper aims to describe two Web-based technologies of geographic information systems (GIS) to be used in monitoring and analysis of environmental processes, proposed by the authors. The technologies analyze the temporal aspect of the process together with the spatial aspect, which defers them from most other works on environmental processes, as these are usually limited either to spatial statistics or to temporal statistics. The approach is instrumental in dynamically finding the relationships between the processes and predicting critical incidents.

Design/methodology/approach – Often, the study of natural processes is limited to the analysis of their spatial properties presented by individual time series. The principal idea of this approach consists in supplementing this traditional analysis with the analysis of time fields. In this way, the authors are able to analyze temporal and spatial properties of environmental processes together.

Findings – The paper presents two technologies which provide the analysis of spatial and temporal data obtained in natural environment monitoring. The discussed spatio-temporal data mining methods are shown to enable the research into environmental processes, and the solution of practical issues of critical situation forecasts.

Originality/value – The paper discussed Web-based GIS technologies for the analysis of the temporal aspect of the environmental process together with the spatial aspect. Application examples demonstrate the ability of this approach to find the relationships in dynamics of the processes and to predict critical incidents.

Keywords Environmental monitoring, Earthquake prediction, Emergency oil spill, Geoinformation analysis, Spatio-temporal processes

Paper type Research paper

1. Introduction

Systems of monitoring of natural processes operate with spatial and spatio-temporal data. The specific character of these data and the increasing complexity of their joint analysis require special techniques and technologies, which are implemented in Web-based geographic information systems (GIS).

The data that involve natural processes are distinguished by large volume and dynamic character. In many cases, the tasks of analysis and forecasting require intensive computations of such data both locally and on remote servers. For this reason, GIS that monitor and analyze natural processes must be able to perform, in addition to standard

A shorter version of this paper was presented at the 15th International Conference on Computational Science and Its Applications, ICCSA 2015 (Gitis *et al.*, 2015).

The research is supported by the Russian Science Foundation grant (project 14-50-00150).

International Journal of Web Information Systems
Vol. 12 No. 1, 2016
pp. 102-124

1744-0084
DOI 10.1108/IJWIS-10-2015-0032

operations, such functions as input and integration of large volumes of data from remote servers and local networks; interactive visual exploration, including animated cartography; spatial and spatio-temporal modeling, data mining and forecasting; and submitting job forms and starting intensive calculations on remote servers.

Web-based geographic information technologies for environment monitoring are implemented using client-server architecture with thin or thick clients. As a rule, thin client technologies are applied to allow the user to view the results of process modeling in a geographical context. Some examples of this technology can be found in the works on marine pollution monitoring and forecasting (Hamre *et al.*, 2009; (Kulawiak *et al.*, 2010). Thin client technology for environmental process monitoring has two limitations. On the one hand, the user needs to access a server for any operation, including the simplest visualization, which renders interactive data analysis almost impossible. On the other hand, such solutions do not support joint analysis of the data received from the remote servers and the user's confidential data stored in the local network. Thick client technologies overcome these limitations. As a rule, the solutions are implemented as Java applications. An example of such a technology designed for environmental monitoring and natural resource management is given in Tsou (2004).

Often, the study of natural processes is limited to the analysis of their spatial properties only. In this paper, we present two of our technologies, which provide the analysis of both spatial and temporal data obtained by natural environment monitoring. They are a Web GIS platform working directly with online resources and a Web GIS integrated into a monitoring system. The first technology is designed for monitoring and analysis of seismic fields, while the second one is used in the Unified State System of Information on the World Ocean (ESIMO). Both technologies are based on the methods of spatio-temporal data mining.

The paper is organized as follows. In Sections 2.1-2.3, we describe our approach and the methods of analysis of spatio-temporal processes that have been realized in GIS GeoTime 3. Sections 2.4 and 2.5 contain two examples of application of the methods realized in GIS GeoTime 3. The first example demonstrates that involvement of the temporal component into analysis of GPS data allows finding spatio-temporal relationship between seismicity and horizontal components of surface deformations. The second example demonstrates a method of assessing the quality of earthquake prediction. In Section 3, we present a technology, which combines two ways of environmental data presentation and analysis: visual express analysis available to a wide range of users and comprehensive analysis of spatio-temporal data implemented by specialists. The technology is illustrated by the results of analysis of seismic catalogs executed on the Web-based GIS platform. Section 4 describes methods of data analysis using Web-based GIS GeoESIMO incorporated into a large-scale environmental monitoring system. As an example of the application, the results of analysis of the emergency oil spill in Barents Sea are given.

2. Geoinformation analysis of spatio-temporal processes

2.1 GeoTime approach

Environmental monitoring and assessment are being applied for systematic estimation, analysis and forecasting of natural processes. GIS is being used for visualization and study of space structure and time behavior of natural processes, for detection of abnormal changes, prediction of natural catastrophes and decision support.

In 1991, a desktop version of GIS GeoTime has been developed in Gitis *et al.* (2004). It was implemented for the study of pre-earthquake processes. In 1990s, detection of earthquake precursors was based on the analysis of time series referring to seismotectonic characteristics in a fixed space domain (the simplest example is the time series of density of earthquake epicenters within some area) and geo-monitoring time series, averaged over the stations in the domain. Such sort of analysis disregards spatial heterogeneity of the seismotectonic data. GIS GeoTime was the first system implementing the detection of earthquake precursors on the base of time-dependent fields, i.e. functions defined on 3D space (two spatial and one time coordinates) rather than one-dimensional time series.

Web GIS GeoTime 3 (www.geo.iitp.ru/GT3/) expands the ideas of the desktop version (Gitis *et al.*, 2012), (Metrikov *et al.*, 2011). It is implemented as a Java application and loaded via Java Web Start. The system can dynamically load distributed data and plug-ins, run remote computing and store the user output. GeoTime 3 supports parallel multithreaded data processing on multiprocessor/multicore front-end computers.

GIS GeoTime 3 processes the data presented in coordinates X,Y,Z,T, where X and Y are geographic coordinates, Z is the altitude (or depth) and T is the time coordinate. Continuous entities are represented as functions defined on regular 2D, 3D and 4D grids. The functions can take either scalar values or 2D or 3D vector values. Scalar 2D fields are represented as functions of two arguments, 3D fields as functions of three arguments, including depth and time, 4D field as a function $f(x,y,z,t)$. Vector 2D and 3D fields are vector-functions with components directed along the geographical coordinate system axes: $\mathbf{s} = s_x(x, y)\,\mathbf{x} + s_y(x, y)\,\mathbf{y}$, $\mathbf{v} = v_x(x, y, z)\,\mathbf{x} + v_y(x, y, z)\,\mathbf{y}$, $\mathbf{u} = u_x(x, y, t)\,\mathbf{x} + u_y(x, y, t)\,\mathbf{y}$. Discrete entities present geographical objects as lines, polygons and points. Lines and polygons can be specified in geographical coordinates X, Y or in coordinates X, Y, T. Points present geographical objects in coordinates X,Y, sequences and series of measurements in coordinates X, Y, Z and X, Y, T, catalogs of events in coordinates X, Y, Z, T. Attributes of objects can be presented as numbers, vectors or text. Coordinates and attributes of objects are assigned to their descriptors and may be changed in space and time. In visual analysis, raster and tile maps can also be used.

As various characteristics of spatio-temporal processes are presented by data of different types, to operate with different properties of the processes, we need to fulfill operations of converting and transforming the data. GeoTime 3 allows the following transformations of the geoinformation layers: from vector to grid representation and vice versa, from 3D to 2D and from 4D to 3D layers. In simple cases, the system itself analyzes the types of layers and the coordinate binding and then offers the user a set of allowed operations and the default values of the processing parameters. In this sense, the tools of GeoTime 3 are universal with respect to data type.

2.2 Visual exploration

Visualization tools are intended to simplify the visual perception of the geographical information and provide a concise and descriptive data representation in response to a user's information need. It deals with managing display parameters, constructing illumination model of the surface, plotting the cross-section of any grid-based layer along a user-defined profile, browsing through the values of any grid-based layer, retrieving subsets of vector objects via SQL-like request, reading attributes of any vector-based object, etc.

Display parameters of the thematic data properties are filling of the layer, color, thickness and style of lines, type and size of icons and label style. The parameters depend on numeric or nominal values of the layer.

Scalar 2D field is displayed as a map in a corresponding coordinate plane. Scalar 3D and 4D field can be presented in all the 2D coordinate planes. The system supports animation to visualize the changes in the field on the third coordinate. The animated maps may be saved as GIF or AVI files.

Vector 2D and 3D fields can be visualized as arrows in the geographic coordinate plane XY. Visualization of 3D fields is realized with the help of animation varying the values of the field along z (respectively, T)-axis.

In some applications, one needs to carry out a visual analysis of a point field (catalog) of events. In general, catalog of events is a marked discrete subset of a 4D space X, Y, Z, T. As a rule, a mark corresponds to the magnitude of the event. Visualization of the event field is supported by animation in the coordinate planes XY, XZ, XT, YZ, YT, ZT. Visual analysis of relation between several processes is supported by synchronous animation of multiple layers and interactive construction of combined plots.

The local properties of the processes specified by scalar 3D fields, catalogs of the events and numeric series could be visualized using plots. For any point (x^*, y^*) in the geographic coordinate plane, the plot shows the dependence of the field (or series) value on depth (respectively, time). For a catalog, the plot shows the time sequence of magnitudes of events in a circle of a certain radius with the center (x^*, y^*). The position of the reference point (x^*, y^*) is dynamically controlled by the cursor.

Measurements in GeoTime 3 are presented by operations of several types using an interactive graphical interface. A class of available standard operations includes computation of a distance between points, computation of a polygon area, reading the attributes of vector objects and measurement of the values of function depicted on the plots. For scalar fields, there are measurements of two types: the measurement of the layer value at any point and the evaluation of the elementary layer statistics in a simply connected polygon. For a 2D field, the system just measures the value at a given point, while for 3D fields, it is possible to display the dependence of the measured values on depth or time. In addition, in the geographical coordinates, it is possible to visualize and measure the values of a cross section of 2D field along an arbitrary profile. The dynamism of all measurements is provided by interactive control of the position of the point, polygon shape and the choice of the profile.

2.3 Spatio-temporal modeling techniques

Modeling techniques make it possible to carry out a joint analysis of data presented in various formats and allow the researcher to extract new information from thematic, spatial and spatio-temporal properties of the data.

2.3.1 Data conversion. Converting data of different types to a common format, usually to the format of a scalar grid field, allows the user to involve into study several properties of the investigated processes at one time. Moreover, converting extends visual analysis capabilities and makes it possible to combine several map layers in one map and to perform synchronous animation.

Four types of conversion operations are provided by GIS GeoTime 3: interpolation of the values of the layer containing irregular points to get a scalar 2D or 3D grid field,

creation of vector fields out of scalar fields, construction of isolines for scalar 2D and 3D fields and construction of scalar grid fields out of the contours.

2.3.2 Local analysis. A typical technique for the local analysis is calculation in the moving spatio-temporal window. The dimension of the window and its parameters are set by the user within the limits defined by the dimension of the analyzed layer. By default, the result is attributed to the point whose coordinates correspond to the center of the spatial area of the window and the last slice in time.

There is a set of predefined operators, which can be applied to a scalar field in a moving window. There is also a possibility for the user to construct a new operator. The predefined operators compute the illumination model for the layer; mean, median, standard deviation, the difference between the value in the center of the window and the mean value in the window; maximum, minimum and difference between maximum and minimum; the module and the azimuth of the gradient of 2D slice; and the curvature of the isolines of a 2D slice in the XY plane. The user can compute a convolution of the input field with an arbitrary spatio-temporal kernel.

For two scalar 2D, 3D or 4D fields the layer of values of correlation coefficients between these fields in a moving (2D, 3D or 4D, respectively) window can be calculated. When the initial fields are of different dimension, an automatic cloning of field values for the missing coordinates is performed. In addition, the fields can be adjusted to a uniform grid. By default, the minimum grid spacing in each coordinate is set.

Calculations in a moving window are also used to create a scalar field from the vector layers of lines and points, for instance, the field of object density, the field of distances from objects to the grid nodes, etc. In this case, the dimensionality of the output scalar field is equal to or less than the dimensionality of the input vector layer.

Applied tasks of spatio-temporal analysis require sometimes to estimate the similarity of the behavior of a process in different geographical locations. The similarity of the 3D scalar field $f(x, y, t)$ at two points, (x^*, y^*) and (x, y), can be defined as the correlation coefficient $\mathrm{cor}(f(x^*, y^*, t), f(x, y, t))$ of the corresponding time series (similarly for a 3D $f(x, y, z)$ field). The result of the analysis is a 2D field of correlation coefficients.

The user can easily interpret the results of estimating the local similarity of geographic points made on the basis of several 2D fields. The simplest measure of similarity is the distance function. Let to each point (x, y) in the map, a vector $\mathbf{f} = (f_1, f_2 \ldots, f_l)$ of thematic field properties be assigned. Then, the similarity is defined as a function of distance in the space of thematic properties: $S = 1\text{-}\rho(\mathbf{f}^*, \mathbf{f})/R$ if $\rho(\mathbf{f}^*, \mathbf{f}) < R$ and $S = 0$ if $\rho(\mathbf{f}^*, \mathbf{f}) \geq R$, where R is chosen by the user (typically, when calculating the similarity, the values of thematic properties are normalized by standard deviation). The 2D scalar field of similarity is a field in the geographic space XY.

2.3.3 Integral analysis. A typical technique of integral analysis is grid-based computing. The results of operations are scalar grid-based fields, which characterize the properties of environmental processes.

In many applications, it is important to compile a scalar field, which is a function of one or more input fields. GeoTime 3 contains a predefined set of functions; in addition, a function can be constructed by the user from a set of elementary functions using algebraic and logical operations.

Fields of different dimensions and with different grid spacing may be involved in one and the same operation – they are just converted automatically to the same dimension and to uniform coordinate grid.

An important operation of grid computing is the scalar field projection. The operation consists in calculating fields of a smaller dimension, whose values are elementary statistics of the source field along the projection axis. For example, for a scalar 3D field $f(x, y, t)$, it is possible to calculate 2D fields of mean values of $f(x, y, t)$ along the axis T, Y or X, similarly for a 4D field.

The estimation of spatial similarity of two 3D fields belongs to the same sort of operations. The result is a spatial 2D field whose values are determined by the measure of similarity of corresponding time or depth series.

2.4 Modeling and analysis of earthquake precursors

2.4.1 Tools and techniques. Support of the research in the domain of natural hazard prediction is one of the most important applications of dynamic GIS. GIS GeoTime 3 is to a large extent focused on the analysis of earthquake precursors (Gitis *et al.*, 2012). The analysis is based on the assumption that the process of earthquake preparation is accompanied by spatio-temporal anomalies of characteristics of the geological environment in the vicinity of a future event. These anomalies are associated with the accumulation of potential energy and a gradual transition of the geological environment from the phase of elastic deformations to the phase of plastic deformations.

GIS GeoTime 3 provides a three-stage analysis of earthquake precursors by retrospective data assessing the dynamic characteristics of the seismic process, detecting spatio-temporal anomalies of seismic process (change-point detection) and assessing the quality of earthquake precursors.

2.4.2 Assessing the dynamic properties of the seismic process. To support the study of seismotectonic properties of the geological environment, GeoTime 3 calculates spatio-temporal fields (3D feature fields) from earthquake catalogs and geo-monitoring time series. To this end, we use the local kernel techniques, adaptive weights smoothing (Goldenshluger and Spokoiny, 2006) and interpolation methods.

2.4.3 Detection of spatio-temporal anomalies of seismic process. It is assumed that the geological environment is heterogeneous in space, but in the normal state, it has stationary dynamics, which is perturbed during the preparation of geological catastrophe. The task of finding out the anomalies is reduced to the problem of change point detection in a random process. In GIS GeoTime 3, several parametric models for the detection of spatio-temporal anomalies in the feature fields are realized. In fact, there are no substantial reasons for adopting a parametric model, as the distribution of the process is unknown and cannot be obtained on the basis of the available information. Therefore, nonparametric approach to the problem of change point detection is more promising.

2.4.4 Assessing the quality of earthquake precursors. To test the quality of earthquake precursors, we apply an earthquake prediction algorithm to retrospective data: the better earthquake prediction accuracy, the better the earthquake precursor subjected to the given forecasting rule. Our forecasting rule announces an earthquake alarm at some grid point (x, y, t) if the value of the earthquake precursor at this point satisfies a certain condition. If the alarm is announced, the *alarm area* is constructed in the form of a cylinder whose base is a circle (on the spatial slice) of radius R centered at (x, y, t), and the element is directed along the time coordinate and its length is equal to T.

The forecast is successful, if the earthquake epicenter falls into the alarm area.

To assess the accuracy of a forecast, we use a sample set of the strong earthquakes. The quality criteria of the forecast are the percentage of correctly predicted events (u) and the percentage of the number of grid points in the unification of all alarm areas among the all grid points of the precursor field (v). We call *u the forecast level* and *v the alarm volume*. The quality of the forecast for the analyzed earthquake predictor can be presented as the forecast accuracy function $u(v)$. This function is well known in statistics. It is called the receiver operating characteristic (ROC). Two points of this function are known in advance. The point $u = 0$ per cent and $v = 0$ per cent corresponds to the situation when there is no alarm, and the point $u = 100$ per cent and $v = 100$ per cent corresponds to the situation when the alarms cover all points of the grid. For a given value of the alarm volume, V, the greater the integral of the forecast accuracy function $U(V) = \int_0^V u(v)dv$, the better the precursor.

2.4.5 Assessing the quality of earthquake prediction. We assume that strong earthquakes may occur in the neighborhood of any grid node in case of the value of precursor field $f(x,y,t)$ in this point is abnormally small (less than a given threshold $\theta_<$) or abnormally big (greater than a threshold $\theta_>$). In GeoTime 3 for tested thresholds $\{\theta_<\}$ and $\{\theta_>\}$, the forecast accuracy functions are calculated, $u_<(v)$ and $u_>(v)$, respectively. In addition, a function $u_{opt}(v)$ of the forecast accuracy for the optimal decision rule using both thresholds is calculated: alarm is declared if $(f(x, y, t)<\theta_<) \in (f(x,y,t)>\theta_>)$. To find the function $u_{opt}(v)$, we use an algorithm, which finds thresholds $\theta_<$ and $\theta_>$ to obtain the best forecast level u for each value of the alarm volume v.

To assess the predictive power of the precursor field, in GeoTime 3, the integrals of the forecast accuracy are used in addition to the described above functions of the forecast accuracy:

$$U_<(V) = \int_0^V u_<(v)\,dv, \quad U_>(V) = \int_0^V u_>(v)\,dv, \quad U_{opt}(V) = \int_0^V u_{opt}(v)\,dv$$

2.5 Case study: application of GeoTime 3 for assessing the interrelation between two processes presented by time series and marked point field

There are three major objectives of exploring the spatio-temporal dynamics of geographical processes: finding the connection between the different processes, zoning (segmentation) the territory by intensity and types of processes and hazard prediction (Gitis and Derendyaev, 2014). We consider an example of GIS GeoTime 3 application to finding the relationship between the processes of horizontal deformations of Earth's surface estimated by GPS and seismicity. Geodynamic aspects of analysis of mutual influence of deformation of Earth's surface and seismicity are discussed in Sobolev *et al.* (2010). Here, we pay attention to the analytical aspect of the problem, which consists in finding out the interrelation between two natural processes presented by different types of monitoring data. Indeed, Earth's surface deformations are presented by the temporal sequences obtained from GPS stations. Seismic process is represented by an earthquake catalog. Analysis of the relationship between these processes is complicated, as these processes are described by data of different types.

In general, the catalog of events is a marked set of points with three spatial and one temporal coordinates. In our case, the mark corresponds to the strength of event: magnitude or energetic class of earthquake. A GIS GeoTime 3 project based on the data

of Bishkek Research Station of RAS[1] is available at www.geo.iitp.ru/GT3/. The earthquake catalog is rather small. It includes only 740 events with the energy from 7 to 13.7 (this corresponds to the interval of magnitudes from 2 to 5.4) for the period 1994-2008. Surface deformations are represented by the temporal sequences of GPS measurements: horizontal components of displacement from South to North (offset Y) and from East to West (offset X), 14 GPS stations, average interval between measurements is 19 days, the total interval of observations is from July 23, 1997 to May 25, 2007.

Baseline data of the project are shown on the map in Figure 1: GPS stations are indicated by white triangles, the earthquake epicenters are shown with yellow circles, the earthquakes of energetic class $K \geq 10$ are shown as large circles, the size of the circle increases in proportion to the force of the earthquake. The polygons A, B and C indicate the areas selected for analysis.

The hypocenters of most earthquakes are located at depths of 5-25 km, while deformations are determined using GPS at the Earth's surface. Mutual influence of these two fields is problematic. Their combined analysis is hampered by two factors: the insignificant number of GPS stations and low seismicity.

Analysis is carried out in two stages: spatio-temporal data mining of the relationship between the fields of the surface deformations and seismicity and estimation of this relationship.

Spatio-temporal data mining in GeoTime 3 is supported by special tools for discovering the relationship between the processes: synchronous animation of several processes presented as 3D point fields, scalar and vector grid fields and interactive synchronous visualization of time series charts, temporal sequences of events and statistics of 3D grid-based fields for user-defined spatial areas. To represent spatio-temporal and energetic properties of the seismic flow, we calculate the scalar 3D fields of the earthquake epicenter density and RTL criterion (Sobolev and Tyupkin, 1997), (Gitis and Ermakov, 2004). To represent the properties of the surface horizontal deformations, a number of conversions of the GPS time sequences are carried out. First, in our case study, two time sequences of horizontal components of the displacements were interpolated in time series with temporal intervals of 10 days. Next, the time series were interpolated in two spatio-temporal fields with 3D grid cell size of 0.02° latitude × 0.02° longitude × 10 [day] time. Thereafter, the fields were smoothed with a Gaussian kernel function with 3D window width equal to 5 km and 180 days. In a next step, the fields of velocity components V_x and V_y of the horizontal displacements were calculated

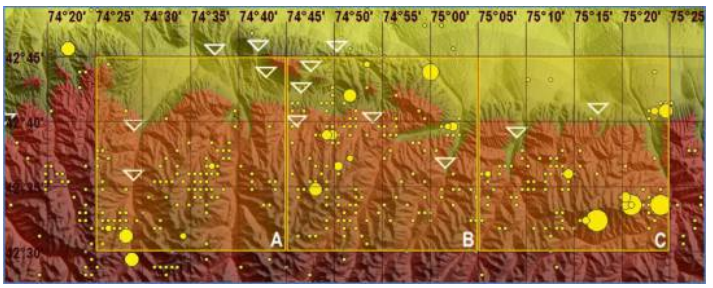

Figure 1.
Map of baseline data

with respect to time. Next, 3D vector field of velocity V was calculated from the velocity components. Further, this field was used only for animated visual exploration.

Synchronous visualization of 3D vector field of velocity, scalar seismic fields of earthquake density and RTL and point fields of earthquake epicenters demonstrates the following: on average, the surface displacements were directed to the northeast at angles of 23-45° relative to the direction to the north and with speeds of 1.4-3.2 mm/year; and the increase in seismic activity culminating in strong earthquakes was accompanied by the growth of the gradient in the field of movement velocities.

The particularity in movements may be quantitatively estimated by the variations in the gradient of the amplitude and direction of the velocity $\mathbf{V}$ in the assigned areas of the Earth's surface. To do this, 3D scalar fields of divergence div$\mathbf{V}$ and curl, curl$\mathbf{V}$, were calculated:

$$\mathrm{div}\mathbf{V} = \partial \mathrm{V_x}/\partial \mathrm{x} + \partial \mathrm{V_y}/\partial \mathrm{y},$$

$$\mathrm{curl}\mathbf{V} = \partial \mathrm{V_x}/\partial \mathrm{y} - \partial \mathrm{V_y}/\partial \mathrm{x}.$$

With the unavailability of values for the vertical component of the Earth's surface movement velocity, the parameter div$\mathbf{V}$ indicates the relative contraction or extension of a small horizontal area near the point of the spatio-temporal raster. This scalar value is independent of the selected coordinate system. Under the same condition (unavailability of values for the vertical component of the Earth's surface movement velocity), the parameter curl$\mathbf{V}$ indicates the rotation of a small horizontal area around the vertical axis. The vector (ort) of this value is directed orthogonally to the horizontal surface of the Earth, upward or downward, depending on the clockwise or counterclockwise mode of the area's rotation. In the general case, the value of the parameter curl$\mathbf{V}$ should change when the center of the coordinate system relative to which the calculations are performed also experiences displacement and rotation.

Quantitative evaluation of the relationship between processes of deformation and seismicity is implemented for the polygons A, B and C shown in Figure 1. Further, we superposed plots of the average values of fields curl$\mathbf{V}(t)$ and temporal sequences of the earthquakes with the energy class $\mathrm{K} \geq 10$ in the polygons A, B, C. It turned out that for all the polygons, the majority of the epicenters of the earthquakes fall in half-yearly intervals, built around significant extrema of curl$\mathbf{V}(t)$. Extrema with amplitude less than 1/5 of the maximal extremum of curl$\mathbf{V}(t)$ in the polygon was considered as insignificant.

Observation interval is determined by the GPS data from July 23, 1997 to May 25, 2007, that is, 9.839 years. Earthquakes of class $K \geq 10$, with the epicenters in the three selected polygons are incompatible events. Therefore, to analyze the relationship between curl$\mathbf{V}(t)$ and earthquakes throughout the region, it can be assumed that the experiment was performed for one polygon within three consecutive temporal segments. Then, the total time of observations is $T = 9.839 \cdot 3 = 29.517$ years, and the total time of intervals around the extrema equals $t = 10$ years. During the observation period, $N = 23$ earthquakes occurred in the polygons. Of this number, $n = 15$ events occurred in the intervals of extrema.

Consider two hypotheses:

H0. The number of events has the binomial distribution with probability $p = (T\text{-}t)/T = 0.661$, $q = 1\text{-}p = t/\mathrm{T} = 0.339$. The alternative hypothesis:

H1. $q > 0.339$.

To test the hypotheses, we use statistics $\nu = n - Nq/\sqrt{Npq}$, which has a standard normal distribution. If *H0* is true, $\nu = 2.735$. The distribution function $F(\nu = 2.735) \approx 0.997$; therefore, *H0* is rejected with a significance level of 0.3 per cent. This means that with the probability of more than 99 per cent, *H1* may be accepted: strong earthquakes not by chance occurred during the periods of extreme values of curl**V**. Analogous results îf estimation of the relationship between the field of surface deformation and seismicity are obtained for the field div**V**(*t*).

Note that a large number of earthquakes in the area of extremes of curl**V**(*t*) occurred prior to the extrema. Therefore there is no reason to assume that the appearance of an extremal value of curl**V**(*t*) is a reliable sign for earthquake prediction. Perhaps predictive probability can be estimated under more long and extensive observations.

2.6 Case study: assessing the predictive power of the earthquake precursors

We analyzed the earthquake catalog of California. It was downloaded from the site of National Earthquake Information Center (NEIC). It covers the region with coordinates from −124 to −115° W and from 30 to 45° N, and the period from January 01, 1995 to August 13, 2015. The catalog contains 10,363 events with magnitude from 3 to 7.2 and with the depth of the hypocenters up to 67.5 km. Figure 2 shows the maps of earthquake epicenters. The Map 1 shows all epicenters of the region taken from the NEIC data; the region is highlighted by the gray color. The seismically active area, in which during 1995-1996 at least one earthquake with the epicenter inside a circle of radius 100 km is registered, is under consideration. The epicenters from January 01, 1995 to December 31, 1996, are shown at the Map 2; the seismic area under study is highlighted by the gray color. Prediction of strong earthquakes was performed by 3D fields that were limited to this seismically active area. To test the prediction power of an earthquake precursor, the earthquakes that occurred in the period from January 01, 1997 to August 13, 2015, with a magnitude greater or equal to 5.5 are taken. These 23 epicenters are shown on the Map 3. We can see that one of the epicenters not hit in a seismically active zone. Therefore, analysis of earthquake precursor is performed only for 22 epicenters.

The following precursors have been analyzed:

- $\mathbf{f_1}$: 3D RTL field (Sobolev and Tyupkin, 1997), (Gitis and Ermakov, 2004):

$$RTL(x,y,t) = \\ = \frac{1}{\frac{\pi R^2 \varepsilon^2}{1000} \cdot \frac{T\varepsilon}{365}} \cdot \sum_n \left[(E_n)^\alpha * \exp\left(-\left(\frac{r_n}{R} \right)^{pow\_R} \right) * \exp\left(-\left(\frac{t_n}{T} \right)^{pow\_T} \right) \right] \\ * 1\left(\varepsilon - \frac{r_n}{R} \right) * 1\left(\varepsilon - \frac{t_n}{T} \right) \quad (1)$$

where x, y, t are the coordinates of a point on a 3D grid, $1(w) = \begin{cases} 1, w \geq 0 \\ 0, w < 0 \end{cases}$, n is the number of the events, $E_n = 10^{a+bm_n}$ is the energy of the n-th earthquake; m_n is its magnitude; r_n [km] is the distance from the grid node to the event; $t_n \leq t$ [day] is the time interval

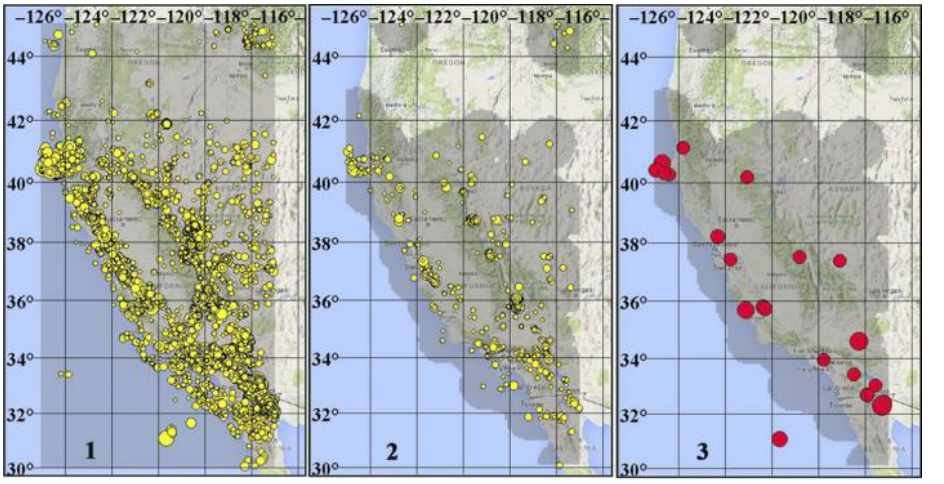

Figure 2.
The earthquake epicenters and the areas under study

Notes: (1) Earthquake epicenters from January 01, 1995 to August 13, 2015, with magnitude from 3 to 7.2, gray color is the area with coordinates from −124 to −115° W and from 30 to 45° N; (2) earthquake epicenters from January 01, 1995 to December 31, 2016, and seismic area under study; (3) the epicenters of strong earthquakes with magnitude more or equal than 5.5 from January 01, 1997 to August 13, 2015

between the grid node and the event, $t_n \leq t$; the following parameters were chosen: $a = 4, b = 1.8$, $\alpha = 0.33$, $\varepsilon = 2$, $R = 50$ km, $T = 50$ days, $pow\_R = 2$, $pow\_T = 1$.

- $\mathbf{f_2}$: The field of anomalies of RTL is calculated as the Student's statistics:

$$t_{st} = (A_2 - A_1)\sqrt{\frac{n_1 n_2 (n_1 + n_2 - 2)}{(n_1 + n_2)(s_1^2 + s_2^2)}} \tag{2}$$

where n_1 (n_2) is the number of time slices of the RTL field, A_1 (A_2) is the mean value of RTL, s_1 (s_2) is the sum of the squared deviations from the mean corresponding to the interval $T_1 = 720$ days ($T_2 = 60$ days, respectively). The parameter values are: $n_1 = 36$ is the number of temporal slices for estimation of the statistics of the RTL field in the background window, $n_2 = 3$ is the number of temporal slices for estimation of the statistics of the RTL field in the test window. If the value of t is close to zero, then the mean values of RTL within the intervals T_1 and T_2 can be considered as invariable with respect to the values of standard deviations. The bigger the value of $|t|$, the more confidence that RTL in the interval T_2 is significantly changed comparing to the interval T_1:

- $\mathbf{f_3 = f_1}$ if $\mathbf{f}_2 > 0$ and $\mathbf{f}_3 = \mathbf{f}_2$ if $\mathbf{f}_2 \leq 0$.

All the fields are calculated with a grid cell size of 0.1° longitude × 0.075° latitude × 20 days. The alarm areas have cylindrical shape with the radius $R = 15$ km and duration of 500 days.

Figure 3 shows the graphical window tab of GIS Geo 3 with a chart for the ROC of the precursor **f**3. The alarm volumes 5.4, 7.8 and 13.6 per cent correspond to the forecast levels 52.4, 61.9 and 71.43 per cent of events, respectively.

3. Environmental monitoring and analysis using Web-based geographic information systems platform

A number of Web sites publish observations on the environmental processes in the form of coordinate time series, temporal sequences of events and time-dependent fields. In particular, the global data centers and regional seismological centers publish real-time earthquake information: the coordinates of the epicenter, the depth of the hypocenter, the time and magnitude, seismograms and other characteristics. From these data, one can calculate physical fields that characterize the spatio-temporal behavior of the seismic process. We consider the field of seismic activity (seismic activity is equal to the number of earthquake epicenters in a certain magnitude interval that occurred in a spatio-temporal window of 1,000 sq. km in space and one year in time). This field characterizes accumulation and release of seismic energy and the changes in the geological environmental structure at different stages of tectonic process.

Considering the fields of seismic activity in the present with respect to the fields of the background seismic activity in the past, one can determine statistically significant regions of seismic quiescence, respectively, seismic activation. The decrease in seismic activity indicates the process of accumulation of seismic energy, while the increase in activity indicates the activation of the seismic process. It is known that both mentioned spatio-temporal anomalies can be precursors of strong earthquakes.

Monitoring technology is realized on a Web platform that consists of two GISs: SeismoMap and GeoTime 3. GIS SeismoMap is realized in thin-client-server architecture based on Google Maps API. It supports express analysis of seismic process and is intended both for specialists and for a wide range of Internet users. GIS GeoTime 3 is realized in thick Java-based client-server architecture. It is a multifunctional analytic system focused on analysis of spatio-temporal environmental processes and earthquake prediction research. It is intended for specialists in the Earth sciences. Thus, the platform of seismic fields monitoring provides information resources and tools for two-level analysis:

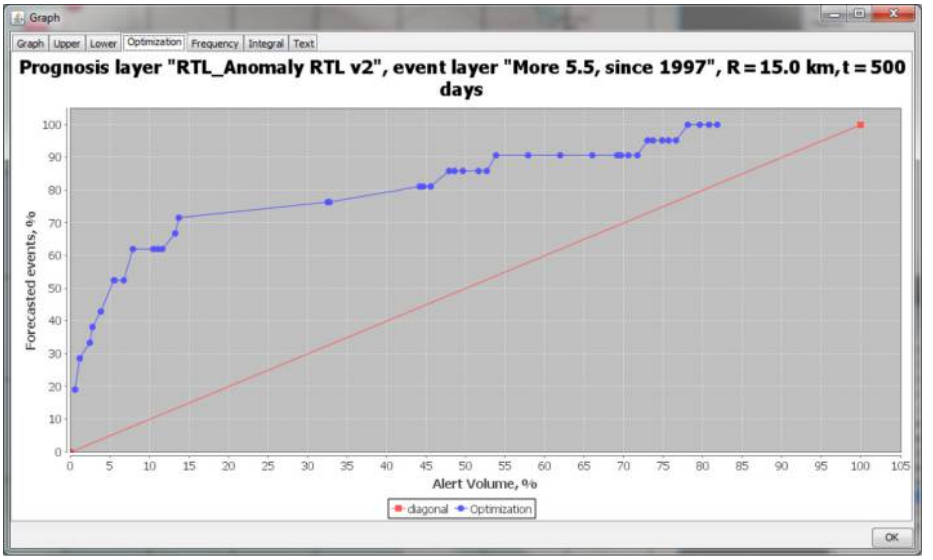

Figure 3.
A tab of GIS GeoTime 3 with the ROC chart for the precursor f3. The alarm volumes 5.4, 7.8 and 13.6 per cent correspond to the forecast levels 52.4, 61.9 and 71.43 per cent of events, respectively

express-analysis of the seismic process accessible to a wide range of users and detailed analysis of the same seismic process, which is performed by specialists.

A prototype of a Web-based GIS platform for monitoring of 24 regions is available at the site of the Institute for Information Transmission Problems RAS http://dcs.isa.ru/geo/2/ and at the site of Kamchatka branch of the Geophysical service of RAS http://saltlab.emsd.ru/server2/.

GIS platform daily loads regional earthquake catalogs for $T_1 + T_2 + T_\varepsilon + T_0 \times N \approx$ 2.5 years from one of the sites http://earthquake.usgs.gov/earthquakes/feed/, www.isc.ac.uk, http://geonet.org.nz or www.emsd.ru/ts/alldemo.php, and calculates the following spatio-temporal (3D) seismic fields: the field of background seismic activity, the field of current seismic activity and the field of changes (anomalies) of the current seismic activity in comparison with the background (the statistical disorder of seismic activity). The algorithm for computing spatio-temporal fields of seismic activity is performed in two steps: estimating a 3D field of density of epicenters for a given representative magnitude and calculation of the 3D field of seismic activity for a fixed b-value in Gutenberg–Richter law, $b = 1$.

Estimation of 3D density field of the epicenters, λ, is performed using kernel methods:

$$\lambda = \frac{1}{\pi R^2 T \mathrm{th}(\varepsilon^2)\mathrm{th}(\varepsilon)} \sum_{m_n \geq m_0} \frac{1}{\mathrm{ch}^2\left(\frac{r_n}{R}\right)^2 \mathrm{ch}^2\left(\frac{t_n}{T}\right)} \tag{3}$$

Here, λ is the value of the density of epicenters at some point, m_n is the magnitude of the earthquake that is greater than the representative magnitude m_0, $r_n < R\varepsilon$ and $t_n < T\varepsilon$ are, respectively, the distance and the time interval between the epicenter of the nth earthquake and the node of the 3D grid, $\varepsilon = 2$, $R = 50$ km, $T = 100$ days. The seismic activity field is calculated for $m_A = 4$ and the magnitude interval $\delta m = 1$ with the help of a standard formula (Kárník, 1971).

To estimate the field of anomalies of seismic activity, we use t-statistics. It is calculated on seismic activity time series at each spatial grid point by the equation (2), where n_1 (n_2) is the number of time slices of the field of seismic activity, A_1 (A_2) is the mean value of seismic activity, s_1 (s_2) is the sum of the squared deviations from the mean, corresponding to the interval $T_1 = 730$ days ($T_2 = 60$ days, respectively).

For each field, GIS SeismoMap visualizes 24 maps of time slices with one-week interval. During the analysis, the user can depict on the map the layer of epicenters of earthquakes that occurred during the time interval of the current seismicity. The interface allows the user to read the magnitude, time and depth of each earthquake. Examples of these maps are given in Figure 4. In the upper parts of Figure 4(a and b), one can see the panels for selection of type and data of the map. Figure 4(c) demonstrates the epicenters of the earthquakes in the past two months prior to the date of the map and the window with attribute values of one of the epicenters.

Now, we are going to give an example of detecting an earthquake precursor using GIS SeismoMap. The earthquake with magnitude $M = 6.1$ occurred on the September 24, 2014, in California. Figure 5 shows a sequence of time slices of 3D anomaly field, which follow at intervals of one week. One can see formation of an anomaly starting from a month and a half prior to the earthquake. Blue tone of the anomalous area denotes that seismic activity is lower compared to the background one. This indicates the accumulation of power. The

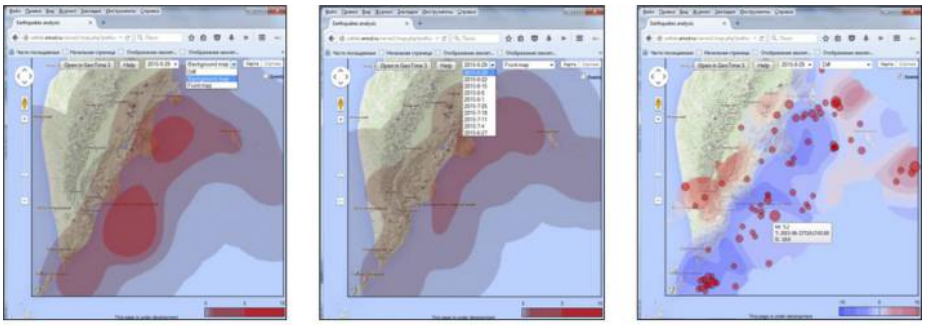

Notes: (a) The map of background seismic activity; (b) the map of current seismic activity; (c) the map of changes in seismic activity

Figure 4.
GIS SeismoMap visualization of time slices of seismic fields corresponding to August 29, 2015

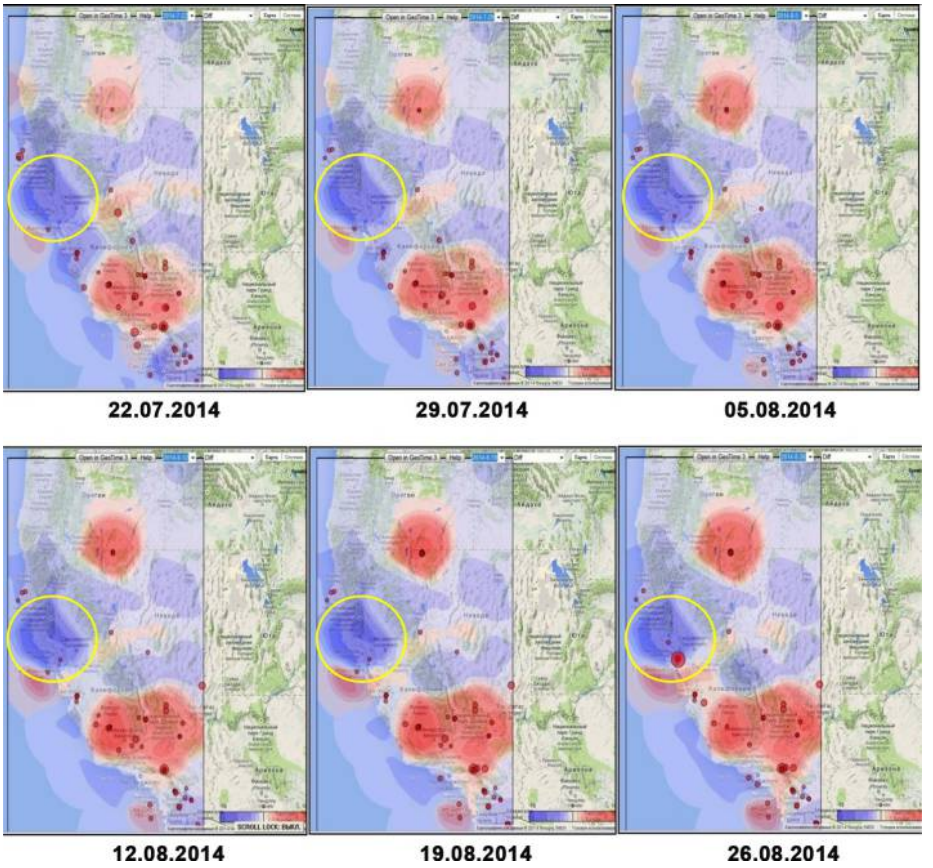

Figure 5.
Time slices of the 3D field of anomalies and epicenters of the earthquakes that took place in the period within two months before the date of the slice. On the slice corresponding to August 26, 2014, in the anomalous area (blue color), there is a large circle that indicates the epicenter of the Californian earthquake with magnitude $M = 6.1$ which occurred on September 24, 2014

following slices demonstrate that the anomalous area decreases and finally converges to the place where later the epicenter of the earthquake appears, which is depicted on the slice corresponding to the date August 26, 2014, as the largest circle.

After reviewing the fields of seismic activity, the user can perform a detailed analysis of the seismic process using GIS GeoTime 3. GeoTime 3 runs with the same seismological and geographic data, which were used to calculate seismic fields in GIS SeismoMap. The tools of GeoTime 3 allow the user to supplement the GIS project with 2D, 3D, 4D grid and vector data from remote or local servers. The results of analysis include the parameters and the fields of earthquake precursors as well as the maps of seismic hazard prediction.

We now consider an example of application of GIS GeoTime 3 for retrospective detection of anomaly that appeared before the earthquake with the magnitude m = 6.8 that took place in Japan on July 11, 2014. The forecast is based on the data from GIS SeismoMap. The earthquake catalog consists of 2,975 events with magnitudes varying from 4 to 7.4 that occurred in the period from January 05, 2012 to July 11, 2014.

Figure 6 depicts six time slices of two fields: the field of epicenters of the earthquakes and the field of the anomalies. An anomaly appeared five months before the earthquake of July 11, 2014. The earthquake epicenters on the map correspond to the moving interval of 30 days. The right boundary of this interval coincides with the time slice of the anomaly field. Yellow circle on the last map is the epicenter of the earthquake under consideration.

4. Data analysis using Web-based geographic information systems incorporated into a large-scale environmental monitoring system

4.1 Geographic information systems GeoESIMO

Web GIS GeoESIMO is incorporated into the ESIMO for the analysis of environmental monitoring data. ESIMO is supported by about 200 databases, http://portal.esimo.ru/portal/. ESIMO's distributed databases contain over 2,300 diverse information resources from more than 80 data providers, of more than 5 TB total size. About 30 per cent of the data is updated with periodicity varying from several minutes to a day. Analytical resources include more than 100 computer systems that are located on servers in different organizations. The technological basis of the ESIMO is service-oriented infrastructure and international standards, ensuring the functioning of the elements and communications of the ESIMO.

GIS GeoESIMO is developed on the base of GIS GeoTime 3. To integrate GIS into ESIMO, a number of additional functions has been brought into development, such as: authorized access to distributed information and computational resources, the preservation of the results of the analysis in the monitoring system for re-use or for transmission to another user, automatic registration of interaction between the GIS components (fault messages, tracking the progress of external tasks and logging GIS operations), the connection of GIS applications to the portal of monitoring systems, creating and editing by the user a problem-oriented GIS-project, etc.

GeoESIMO is connected with the ESIMO portal as a custom portlet. Access to GIS applications through http://portal.esimo.ru/portal/portal/esimo-user/services/geoesimois regulated. Open access is available at the demo Web site www.geo.iitp.ru/esimo

Figure 7 shows the GeoESIMO starting window with GIS-application to the region of the Barents Sea. The map shows the digital elevation model and Russian ships. The data

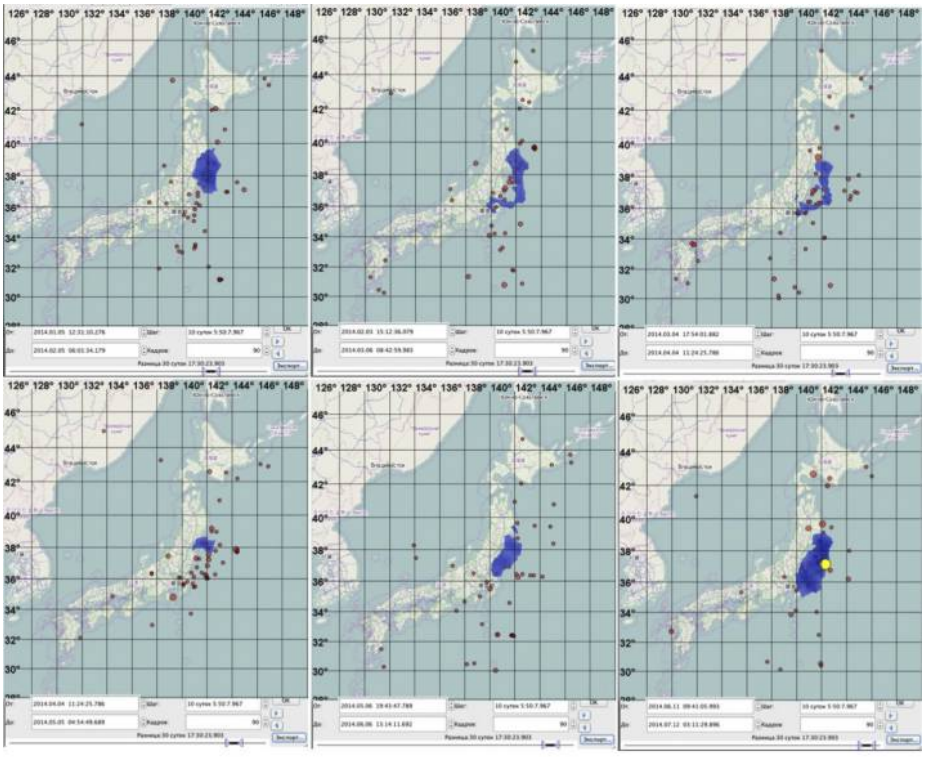

Notes: (1) The anomaly of February 05, 2014, epicenters from January 05, 2014 to February 05, 2014; (2) the anomaly of March 06, 2014, epicenters from February 03, 2014 to March 06, 2014; (3) the anomaly of April 04, 2014, epicenters from March 04, 2014 to April 04, 2014; (4) the anomaly of May 05, 2014, epicenters from April 04, 2014 to May 05, 2014; (5) the anomaly of June 06, 2014, epicenters from May 06, 2014 to June 06, 2014; (6) the anomaly of July 12, 2014, epicenters from June 11, 2014 to July 12, 2014; the yellow circle indicates the epicenter of the forecasted earthquake

Figure 6.
Time slices of the fields of the earthquake epicenters and anomalies. The dates corresponding to the slices from left to right and from the upper row to the lower row

were loaded on December 04, 2014, from the server of the enterprise "Morsvyazsputnik". For illustrative purposes, the data are filtered so that the vessels with the speed greater than 1 knot are presented. The rectangle shows the attributes of the vessel "Norilsk Nickel": the speed equals 12.2 knots, the course is 264, the date and time Thursday, December 04, 12:16.00 GST 2014. To the left of the map, a window of the map layers is depicted, where one can choose to load information resources from Web servers and ESIMO: geodata in different formats, tile maps and maps in the WMS format. Under the layer window a fragment of the visualization attributes control window is shown. Above the layer window, there is a panel of a hierarchical menu that contains the following groups: File operations, Transform operations and modeling, operations of management of the Calculation and Simulation Systems that are performed on remote servers and operations of selecting the Way of visualization of 3D and 4D data. Above

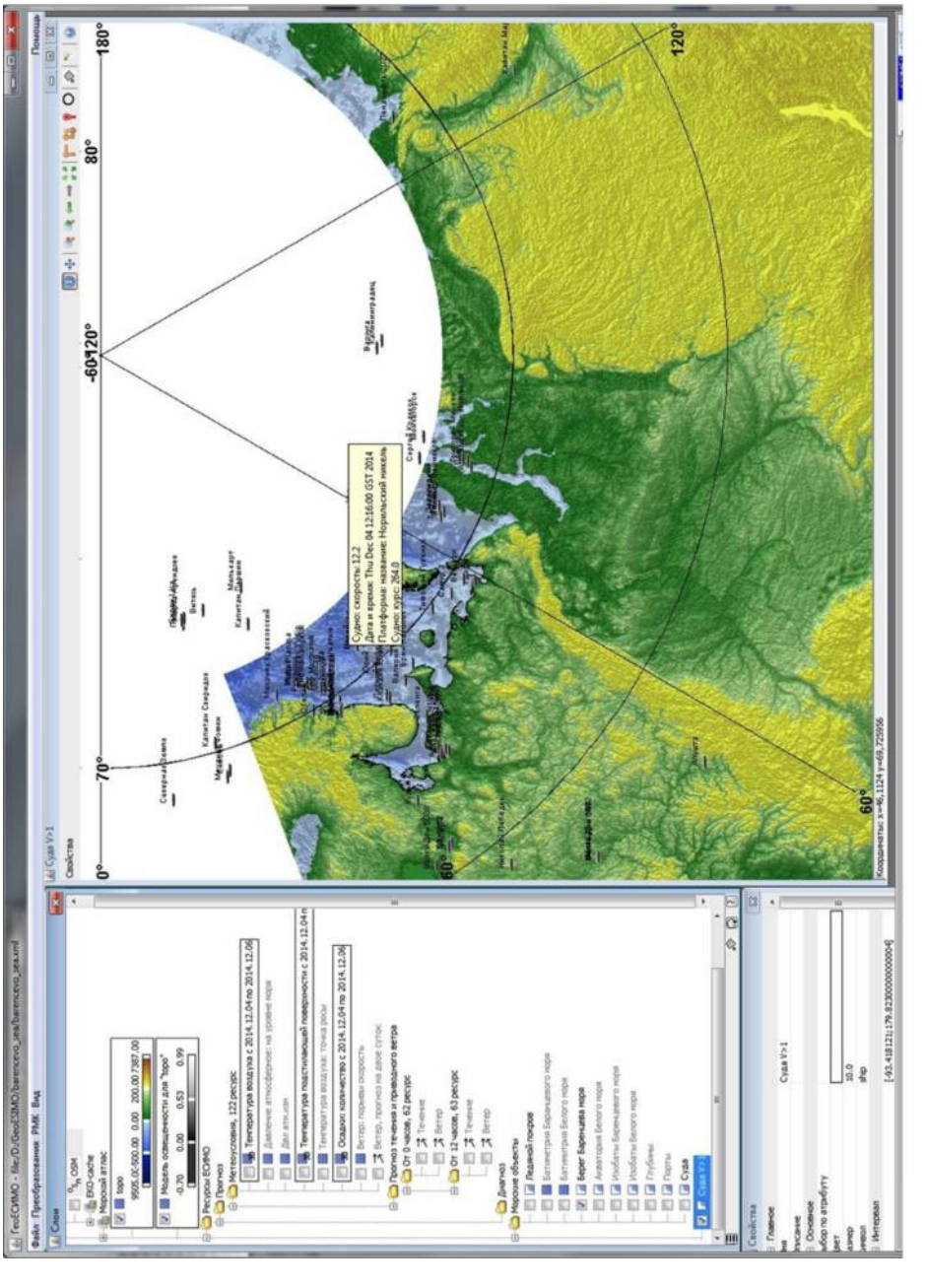

Figure 7.
Starting window of GIS GeoESIMO. The map window shows the digital elevation model and Russian ships with the speed greater than 1 knot. On the left: the window of geographic layers of GIS-project and the window that controls the visualization attributes

the map window, there is a panel that contains the Properties tab, which controls the selection of a map projection and attributes of the grid, and icons that start the operations of visual analysis.

Figure 8 shows a map of the ice conditions (data from the server of Arctic and Antarctic Research Institute). In the rectangular box, one can see the attributes of one of the polygons, which is highlighted in blue.

Figure 9 shows a map of the time slice of the spatio-temporal field of the wind speed forecast at 12:00 on December 4, 2014. On the right, the plots of the time series of forecast for December 4, 2014 – December 6, 2014, at the point 32.56° E and 63.34° N are depicted. The reference point is marked by an arrow. The 3D forecast fields of air temperature, land surface temperature, precipitation and wind speed are loaded from the server of Hydrometeorological Center of Russia.

4.2 An example of the environmental monitoring

As an example of application of GIS GeoESIMO, we describe the scenario of an operator work in an emergency oil spill. User tasks are as follows: to estimate the volume, area and depth of contamination, to provide a forecast for the spread of the oil slick and meteorological forecast; and to decide on the possibility of involvement of the emergency aid in the disaster area and about the appropriate equipment delivery.

To predict the consequences of an oil spill, the server application "Express-analysis of emergency oil and oil products spill" is used. The application was developed in the State Oceanographic Institute (SOI).

The modeling process of a spill consists of three main stages:

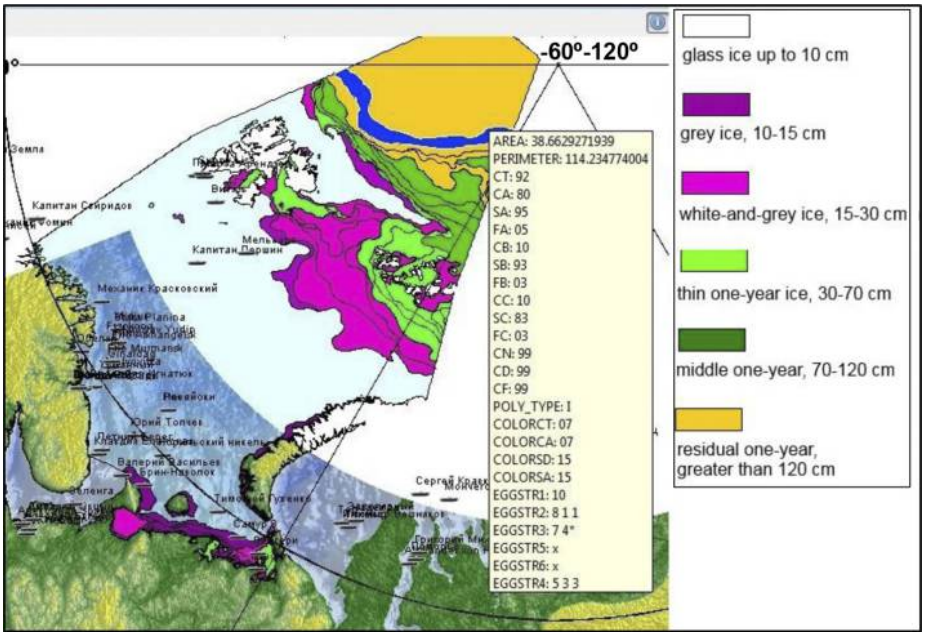

Figure 8.
A map of the ice conditions

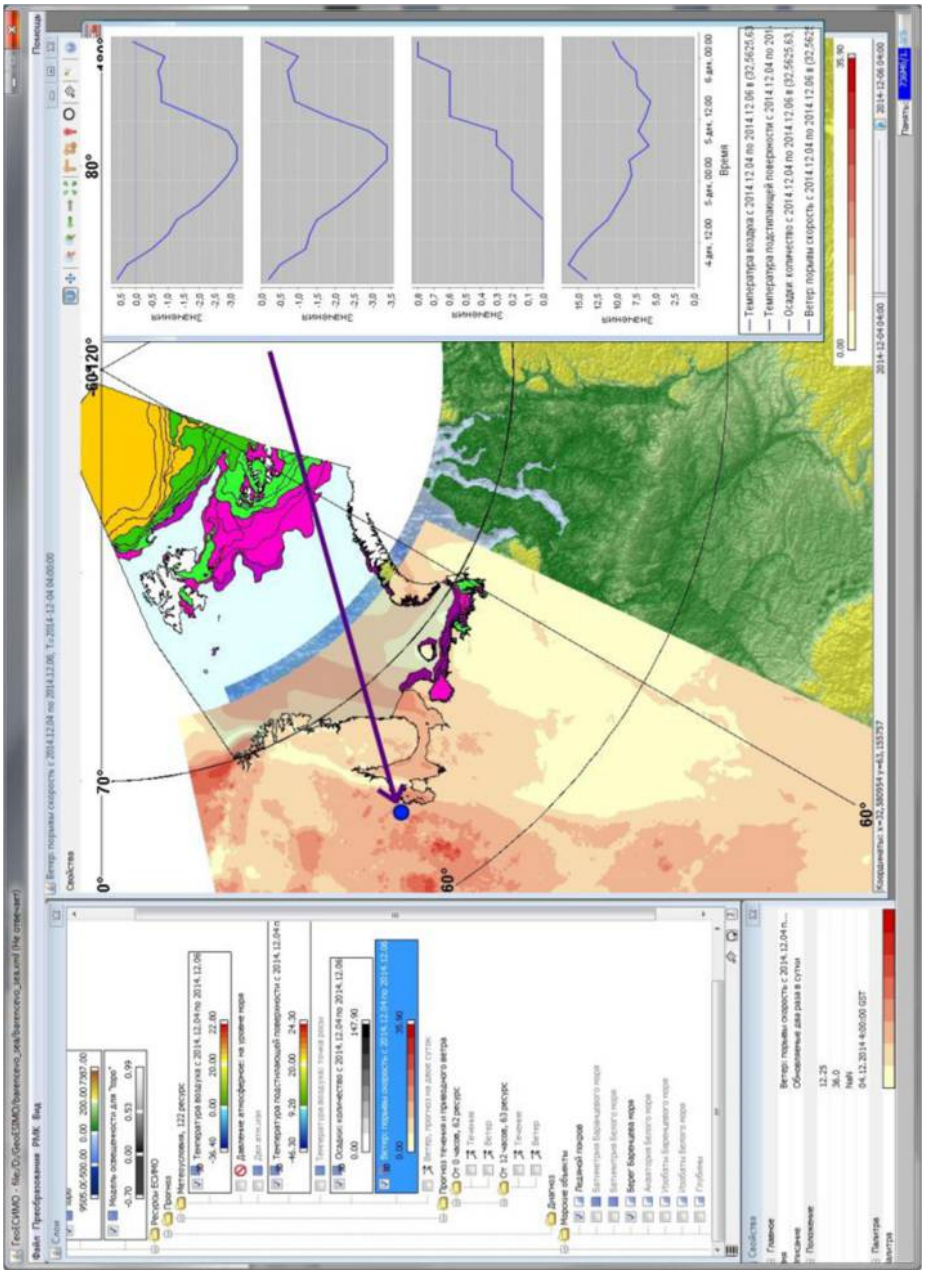

Figure 9.
A map of the wind speed forecast at 12:00 on December 4, 2014. On the right, the plots of the time series of meteorological parameters forecast for December 4, 2014 – December 6, 2014 at the point that is marked by an arrow

(1) *Assignment and transfer of simulation parameters from GeoESIMO to the server of SOI*: In the dialog box of GeoESIMO, the following parameters of the simulation are determined: the duration of the forecast, the iteration step in minutes, the type of the petroleum product, the date and time of the accident, the coordinates of the spill, the intensity and duration of discharge of a petroleum product. Further, the simulation parameters are sent from GIS application through Web service to the server of SOI.

(2) *Computer simulation*: The simulation procedure uses parameters from GIS application, as well as meteorological forecast and other data on the state of the environment. For each simulation step, the coordinates and form of the oil slick for each gradation of oil film thickness, the total mass of spilled oil, the mass of oil on the surface, the mass of evaporated oil, the mass of the oil dispergated into the water and the mass of oil remaining on the shore are calculated. Web service reports on the implementation of each step of calculations.

(3) *Load and aggregation of the results in GIS*: Upon receipt of the notice of completion of the current iteration, GeoESIMO performs the following actions: loads the forecast data (namely, the polygons for three possible values of oil film thickness) corresponding to the completed step of iteration, displays on the interactive map the 3D polygon model of a slick corresponding to the completed step and aggregates the current result with those obtained in the previous steps.

Analysis of oil spill consequences in GeoESIMO is fulfilled basically by cartography tools. The following functions of GeoESIMO are available: animation and step-by-step visualization, reading the attributes, measurement of values, distances and areas, making cross sections, designing of the composition of map layers, creating plots and tables, mapping labels and icons, saving a map with a legend and comments in a Word file, writing the history of the analysis into a file, saving the current session in the form of a GIS project for future reconstruction of the situation, etc.

Figure 10 shows several time slices of simulation of oil slick dynamics. The point of the spill is indicated by "+".

Figure 11 shows several elements of the express analysis of the situation with the oil spill. The point of the spill is indicated by a red circle near the town of Polarny. Purple color represents the oil slick 48 hours after the spill. The figure shows that the oil-spot consists of three polygons. Each polygon delineates the area with a certain thickness of the oil film. The spot area is equal to 27 sq. km. The red line indicates the line segment between the point of the spill and the center of the spot. On the left and on the right are the forecast plots of meteorological parameters in the port of Severomorsk and in the center of the spot of oil, respectively. The plots are constructed by means of GeoESIMO on the query of the server application "Meteograms" of Hydrometeorological Center.

5. Conclusion

Analysis of spatio-temporal processes requires special methods. The principal idea of our approach consists in supplementing the traditional analysis of separate time series with the analysis of time fields. This makes it possible to analyze together both temporal and spatial properties of the environmental processes. To realize this idea, spatio-temporal data mining is needed. In the paper, we have considered the fundamentals of spatio-temporal data mining methods and gave examples of their

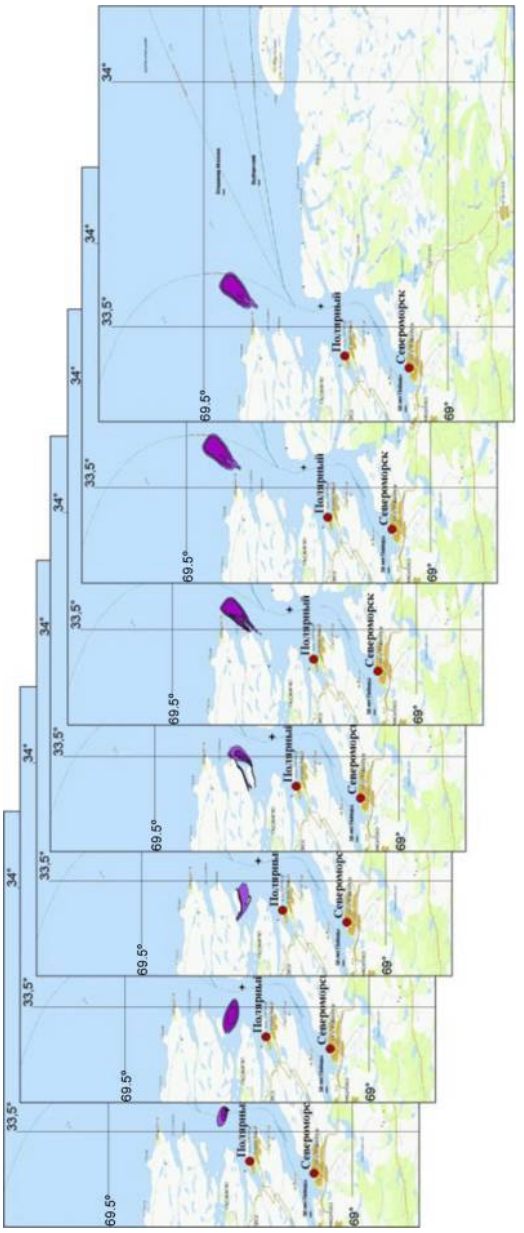

Figure 10.
Time slices of oil slick 2, 6, 12, 18, 24, 30 and 39 hours after the spill

application using GIS GeoTime 3. Methods of GIS GeoTime 3 form the basis of the systems assigned for monitoring and analysis of environmental and anthropogenic processes: Web-based GIS platform, consisting of GISs SeismoMap and GeoTime 3 and Web-based GIS GeoESIMO, integrated into the Unified State System of Information on the World (ESIMO). The use of these systems is illustrated with two case studies.

A Web-based GIS platform is a new technology intended for the analysis of monitoring data on spatio-temporal processes. The platform systematically sends queries to remote servers which receive in real time the results of measurement of various characteristics of the environment and information on the occurring events. Then, the platform converts these data into spatio-temporal fields that describe the state of the environment, evaluate the statistical significance of changes of its properties in space and time and generates a GIS project to run the GIS that supports comprehensive analysis of the data. Thus, the platform provides information resources and tools for two levels of the analysis: visual express analysis available to a wide range of users and sophisticated research implemented by specialists.

GIS GeoESIMO is an example of technology of integration of GIS into a large-scale information system of environmental monitoring. GIS GeoESIMO exploitation shows that the technology, as well as the software, is effective for interactive cartographic representation of distributed dynamic information resources and for advanced analysis of spatial and spatio-temporal information about the situation in the World Ocean.

The examples of the analysis show both techniques, the one implemented as a Web-based GIS platform, and the one integrated into the GIS GeoESIMO, can be used as basic technologies for monitoring and analysis of environmental processes.

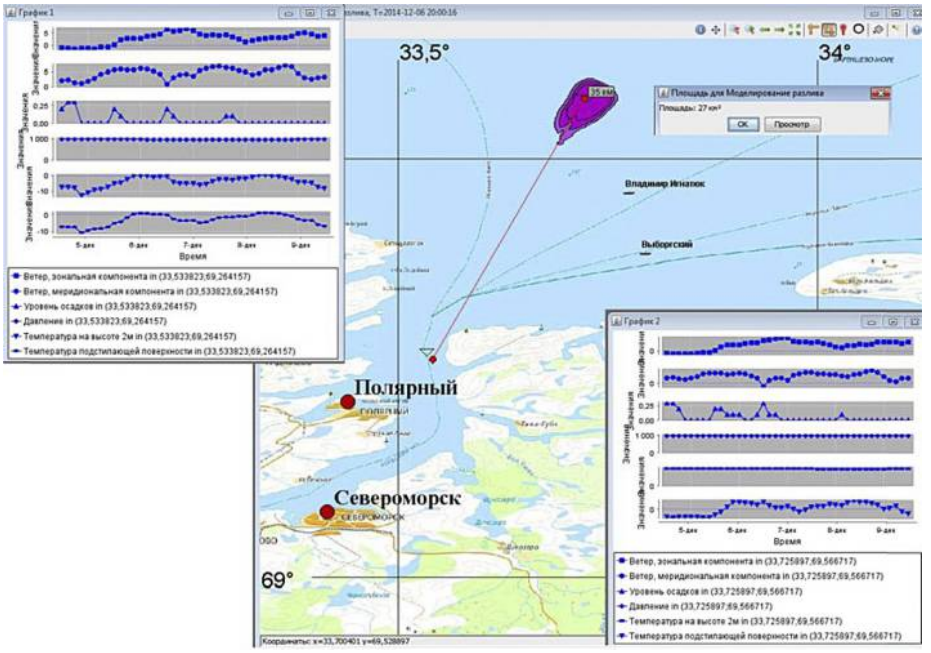

Figure 11. Elements of express analysis of the situation with the oil spill. Red circle indicates the point of the spill; purple polygons demonstrate the forecast position and form of slick for three grades of oil film thickness after 48 hours; on the left and on the right are the forecast plots of meteorological parameters in the port of Severomorsk and in the center of the oil slick, respectively

Note

1. The data have been prepared by the ResearchStation of the Russian Academy of Sciences in Bishkek.

References

Gitis, V. and Derendyaev, A. (2014), "Spatio-temporal analysis of earth's surface deformation by GPS and InSAR Data", Computational Science and its Applications – ICCSA 2014, Springer International Publishing, Vol. 8579, pp. 237-251.

Gitis, V., Derendyaev, A., Metrikov, P. and Shogin, A. (2012), "Network geoinformation technology for seismic hazard research", *Natural Hazards*, Vol. 62 No. 3, pp. 1021-1036.

Gitis, V.G., Derendyaev, A.B. and Weinstock, A.P. (2015), "Web-based geographic information technologies for environmental monitoring and analysis", Computational Science and Its Applications – ICCSA 2015, Springer International Publishing, pp. 698-712.

Gitis, V.G. and Ermakov, B.V. (2004), *Fundamentals of Spatio-temporal Forecasting in Geoinformatics, (In Russian)*, FIZMATGIS, Moscow.

Gitis, V.G., Osher, B.V., Pirogov, S.A., Ponomarev, A.V., Sobolev, G.A. and Jurkov, E.F. (1994), "A system for analysis of geological catastrophe precursors", *Journal of Earthquake Prediction Research*, Vol. 3 No. 4, pp. 540-555.

Goldenshluger, A. and Spokoiny, V. (2006), "Recovering convex edges of an image from noisy tomographic data: information theory", *IEEE Transaction*, Vol. 52 No. 4, pp. 1322-1334.

Hamre, T., Krasemann, H., Groom, S., Dunne, D., Breitbach, G., Hackett, B. and Sandven, S. (2009), "Interoperable web GIS services for marine pollution monitoring and forecasting", *Journal of Coastal Conservation*, Vol. 13 No. 1, pp. 1-13.

Kárník, V. (1971), *Some Characteristics of Seismic Activity*, Springer, Netherlands.

Kulawiak, M., Prospathopoulos, A., Perivoliotis, L., Kioroglou, S. and Stepnowski, A. (2010), "Interactive visualization of marine pollution monitoring and forecasting data via a Web-based GIS", *Computers & Geosciences*, Vol. 36 No. 8, pp. 1069-1080.

Metrikov, P., Derendyaev, A. and Gitis, V. (2011), "Web-GIS technology for dynamic data analysis", *Proceedings of the 2nd ACM SIGSPATIAL International Workshop on Querying and Mining Uncertain Spatio-Temporal Data*, ACM, Chicago, IL, pp. 31-38.

Sobolev, G., Zakrzhevskaya, N., Akatova, K., Gitis, V., Derendyaev, A., Bragin, V., Sycheva, N. and Kuzikov, S. (2010), "Dynamics of interaction between fields of seismicity and surface deformations (Bishkek geodynamic test Area)", *Izvestiya, Physics of the Solid Earth*, Vol. 46 No. 10, pp. 817-838.

Sobolev, G.A. and Tyupkin, Y.S. (1997), "Low-seismicity precursors of large earthquakes in Kamchatka", *Volcano Seismology*, Vol. 18, pp. 433-446.

Tsou, M.H. (2004), "Integrating Web-based GIS and image processing tools for environmental monitoring and natural resource management", *Journal of Geographical Systems*, Vol. 6 No. 2, pp. 155-174.

Corresponding author
Alexander Derendyaev can be contacted at: wintsa@gmail.com